A PHENOMENOLOGICAL STUDY OF THE CONTACT INTERACTION IN FCC-BASED ELECTRON–PROTON COLLIDER

Nur Daif, Güral Aydin †

Department of Physics, Hatay Mustafa Kemal University
31034, Hatay, Türkiye

Received 18 September 2024, accepted 12 March 2025, published online 30 June 2025

In th, and is study, the contact interaction search potential of the FCC-based electron–proton collider was investigated. The study was carried out by using electron–proton collisions at 3.16, 5.0, and 31.6 TeV center-of-mass energies and the cross sections of the collisions were obtained with the package of CalcHEP. The exclusion, observation, and exclusion limits were determined based on a search for deviation of the jet production cross section from the prediction of the Standard Model. The limits on the compositeness scales were obtained for constructive and destructive interferences of four different helicity structures (left–left, right–right, left–right, and right–left). The comparative analysis of the results presented in this study was performed with previous and future prospect collider options. The physics potential of the studied *ep* collider options was evaluated by considering different kinematic cuts and a wide range of luminosity values.

DOI:10.5506/APhysPolB.56.7-A3

1. Introduction

Lepton–hadron collision is a key instrument for obtaining deep information about the structure of matter. In particular, lepton–hadron collisions played an important role in the emergence of the quark-parton model [1]. Achieving high-Q^2 and small Bjorken-x regions is important for understanding the nucleon structure with better precision. Therefore, high-energy electron–proton collisions will provide high-precision information about the quark and gluon structure of the proton. On the other hand, such high-energy colliders will enable the expansion of the Higgs studies and the investigation of New Physics such as quark substructure [2]. Additionally, new particles are likely to be formed in such high-energy colliders. It will also enable the study of New Physics phenomena, including scenarios involving

† Corresponding author: `gaydin@mku.edu.tr`

dark matter. With such colliders, deviations from the Standard Model (SM) can be determined by making precise measurements, and thus New Physics potentials can be investigated.

Research and development of electron–hadron colliders is an ongoing and continuing concern. The energies of the electrons will be limited in circular accelerators due to synchrotron radiation. Therefore, electrons with desired high energy can be obtained by using linear colliders (LC) tangent to circular accelerators. This approach has been considered for different colliders [3–6]. FCC (Future Circular Collider) [7] is the future 100 TeV center-of-mass energy circular pp collider proposed at CERN. In this work, we discuss the physics potentials of the LC $\otimes$ FCC-based ep collider in terms of contact interaction (CI). Firstly, the linear accelerator parameters used in the calculations belong to the PWFA-LC (Plasma Wake Field Accelerator Linear Collider) [8] accelerator, which will enable high energies to be obtained at short distances. The major advantage of a PWFA is that it will allow for building more compact accelerators compared to radio-frequency resonance-based colliders. Secondly, the 50 GeV$\otimes$50 TeVep option which is an initially planned scenario in FCC was considered. Finally, the 125 GeV $\otimes$ 50 TeVep option was considered. Here, the first energy is the electron energy obtained in the linear accelerator and the second is the proton energy obtained in the FCC. The physics limits that can be achieved for different contact interaction scenarios will be estimated. The main goal of this work is to estimate the sensitivity of this New Physics for the specified collider option. In this study, the CalcHEP [9] program, which provides automatic calculation of elementary particle collisions, was used. The contact interaction model is implemented through LanHEP [10], which automates the process of calculating Feynman rules and writing CalcHEP model files.

A considerable amount of literature has been published on contact interactions. In the next part of the manuscript, some published work on the four-fermion contact interaction scale will be reviewed. The search for physics beyond the Standard Model has been realized with high-Q^2 neutral current deep inelastic scattering events recorded with the ZEUS detector at HERA [11]. Two data sets, $e^+ + p \to e^+ + X$ and $e^- + p \to e^- + X$, received between 1994–2000 with the integrated luminosities of $L = 112$ pb^{-1} and $L = 16$ pb^{-1} were analyzed to obtain limits on the compositeness scale in $eeqq$ contact interactions. For contact interaction models, limits ranging from 1.7 to 6.2 TeV have been reported to be obtained on the effective mass scale Λ (*i.e.* the compositeness scale). In another study of [12], lower limits on the compositeness scale were obtained from a general contact interaction analysis. The analysis in that article is based on the full H1 data sample collected in 1994–2007, corresponding to the integral luminosity of $L = 446$ pb^{-1}. In this study, neutral current deep inelastic e^-p and

e^+p scattering cross-section measurements were analyzed to investigate new phenomena mediated by contact interactions. Here, the contact interaction models were examined with the observation of the deviations from the Standard Model expectation at high Q^2. Limits on the parameters of various contact interaction models are presented at the 95% C.L. According to the analysis results, the limits for the general four-fermion *eeqq* contact interaction models were determined between 3.6 TeV and 7.2 TeV, depending on the chiral structure.

In another study, a search was conducted for new resonant and non-resonant high-mass phenomena in dielectron and dimuon final states [13]. In that study, 36 fb^{-1} proton–proton collision data collected at $\sqrt{s} = 13$ TeV by the ATLAS experiment conducted at the LHC (Large Hadron Collider) in 2015 and 2016 were used. Here, the lower limits on the *qqll* contact interaction scale were set between 24 TeV and 40 TeV, depending on the model. Another study used 35.9 fb^{-1} proton–proton collision data collected at $\sqrt{s} = 13$ TeV by the CMS (Compact Muon Selenoid) experiment at the LHC [14]. In that work, a search for physics beyond the Standard Model was carried out based on measurements of dijet angular distributions in proton–proton collisions. In a model in which only left-handed quarks participate, contact interactions were excluded at the 95% confidence level up to a scale of 12.8 or 17.5 TeV for destructive or constructive interference, respectively.

Another study was performed using a 7 TeV proton–proton data sample collected with the LHC CMS detector, corresponding to an integrated luminosity of 5 fb^{-1} [15]. The results of the research on the deviation of the jet production cross section relative to SM are presented. Using the CL_s criterion, lower limits of 9.9 TeV and 14.3 TeV were determined at the 95% confidence level for models containing destructive and constructive interference, respectively. It has been noted that the jet p_t spectrum becomes a competitive observable for investigating phenomena defined by contact interactions. Finally, studies on electron–positron collisions could be carried out for different sources [16–20].

The analysis part of this study consists of two stages. In the first stage, distributions for different kinematic variables were obtained for both SM and different contact interaction models. Thus, deviations from SM were observed. As a result, some cuts were determined to separate the signal from the background. In the second stage, by applying different jet p_t cuts, the deviations of the contact interaction models from the SM were determined with a statistical model over the total cross section. Additionally, bin-by-bin analysis was included in some interaction scenarios. As a result of the analysis, limits for the contact interaction scale are presented for different statistical sensitivities and interaction models. Thus, it was possible to evaluate the sensitivities of different models depending on the transverse momentum cut-off. At the last stage of the study, an uncertainty calculation was made. Changes in the contact interaction scale obtained by the specified analysis method were observed depending on some uncertainties in real detector parameters.

2. Four-fermion contact interaction

If quarks and leptons are made of constituents, then there are new interactions on the scale of the binding energies of the constituents, called the compositeness scale. If the energy of a collider is much smaller than this compositeness scale, strong forces binding the constituents cause flavor-diagonal contact interactions. Contact interactions occur as four-fermion interactions at low collider energies as an effect of fermion compositeness. Therefore, the energy of the collider and the level of compositeness scale are decisive in understanding the substructure of fermions. Contact interactions are suppressed by the inverse powers of the compositeness scale. Most generally, contact interactions are described by the color-singlet chirally invariant flavor-diagonal Lagrangian [21, 22]

$$\mathcal{L} = \mathcal{L}_{\mathrm{LL}} + \mathcal{L}_{\mathrm{RR}} + \mathcal{L}_{\mathrm{LR}} + \mathcal{L}_{\mathrm{RL}}\,, \tag{1}$$

$$\begin{aligned}
\mathcal{L}_{\mathrm{LL}} &= \frac{g^2_{\mathrm{contact}}}{2\Lambda^2}\sum_{i,j}\eta^{ij}_{\mathrm{LL}}\left(\bar{\psi}^i_{\mathrm{L}}\gamma_\mu\psi^i_{\mathrm{L}}\right)\left(\bar{\psi}^j_{\mathrm{L}}\gamma^\mu\psi^j_{\mathrm{L}}\right)\,,\\
\mathcal{L}_{\mathrm{RR}} &= \frac{g^2_{\mathrm{contact}}}{2\Lambda^2}\sum_{i,j}\eta^{ij}_{\mathrm{RR}}\left(\bar{\psi}^i_{\mathrm{R}}\gamma_\mu\psi^i_{\mathrm{R}}\right)\left(\bar{\psi}^j_{\mathrm{R}}\gamma^\mu\psi^j_{\mathrm{R}}\right)\,,\\
\mathcal{L}_{\mathrm{LR}} &= \frac{g^2_{\mathrm{contact}}}{2\Lambda^2}\sum_{i,j}\eta^{ij}_{\mathrm{LR}}\left(\bar{\psi}^i_{\mathrm{L}}\gamma_\mu\psi^i_{\mathrm{L}}\right)\left(\bar{\psi}^j_{\mathrm{R}}\gamma^\mu\psi^j_{\mathrm{R}}\right)\,,\\
\mathcal{L}_{\mathrm{RL}} &= \frac{g^2_{\mathrm{contact}}}{2\Lambda^2}\sum_{i,j}\eta^{ij}_{\mathrm{RL}}\left(\bar{\psi}^i_{\mathrm{R}}\gamma_\mu\psi^i_{\mathrm{R}}\right)\left(\bar{\psi}^j_{\mathrm{L}}\gamma^\mu\psi^j_{\mathrm{L}}\right)\,.
\end{aligned} \tag{2}$$

Here, $\mathcal{L}$ represents the effective Lagrangian, while the indices i and j represent the fermion flavors. Other terms, g_{contact}, Λ and ψ_{LR} represent the coupling constant, compositeness scale, and fermion spinors, respectively. Here, the coupling constant for the new strong interaction is taken as $g^2_{\mathrm{contact}}/4\pi = 1$. Additionally, the terms 'L', 'R' are used to indicate whether the fermion flavor is in the left or right helicity, respectively. In general, in interactions between the same fermion flavors, that is, when $i = j$, these indices are eliminated and only the term $\eta_{\alpha\beta}$ is used. Here, $\eta_{\alpha\beta}$ is called the chirality coefficient. This coefficient is set to ± 1 values as the highest magnitudes and determines whether the fermion scattering amplitude for the contact interactions and SM amplitude interfere constructively or destructively [22].

Contact interactions could occur in two ways. If fermions have common constituents, interchange of these constituents could lead to such interactions. On the other hand, if a quanta pair couple to the constituents of both particles, contact interaction could occur by exchanging the binding quanta. Different contact interaction models are presented as follows, depending on the helicity of the fermion flavors and the type of interference (constructive or destructive)

$$\begin{aligned} \Lambda &= \Lambda^{\pm}_{\mathrm{LL}}\left(\eta^{ij}_{\mathrm{LL}}, \eta^{ij}_{\mathrm{RR}}, \eta^{ij}_{\mathrm{LR}}, \eta^{ij}_{\mathrm{RL}}\right) = (\pm 1, 0, 0, 0)\,, \\ \Lambda &= \Lambda^{\pm}_{\mathrm{RR}}\left(\eta^{ij}_{\mathrm{LL}}, \eta^{ij}_{\mathrm{RR}}, \eta^{ij}_{\mathrm{LR}}, \eta^{ij}_{\mathrm{RL}}\right) = (0, \pm 1, 0, 0)\,, \\ \Lambda &= \Lambda^{\pm}_{\mathrm{LR}}\left(\eta^{ij}_{\mathrm{LL}}, \eta^{ij}_{\mathrm{RR}}, \eta^{ij}_{\mathrm{LR}}, \eta^{ij}_{\mathrm{RL}}\right) = (0, 0, \pm 1, 0)\,, \\ \Lambda &= \Lambda^{\pm}_{\mathrm{RL}}\left(\eta^{ij}_{\mathrm{LL}}, \eta^{ij}_{\mathrm{RR}}, \eta^{ij}_{\mathrm{LR}}, \eta^{ij}_{\mathrm{RL}}\right) = (0, 0, 0, \pm 1)\,. \end{aligned} \tag{3}$$

Here, the value of $\eta_{\alpha\beta}$ being 0 indicates that the corresponding interaction is not included in the presented scenario. Thus, a single $\eta_{\alpha\beta}$ value was retained in each scenario and others were excluded. In this study, purely four-fermion contact interactions of electron-proton collisions were considered. The interactions at large extra dimensions were not taken into account. The basic interaction process in our calculations could be expressed as follows:

$$e + p \to e + j + X\,. \tag{4}$$

Here, the j term refers to the particles of $(j: u, \bar{u}, d, \bar{d}, c, \bar{c}, s, \bar{s}, b, \bar{b}, g)$. The total cross section of this interaction is shown in Eq. (5) [23]

$$\sigma_{\mathrm{tot}} = \sigma_{\mathrm{SM}} - \eta_{ij}\frac{F_{\mathrm{I}}}{\Lambda^2} + \frac{F_{\mathrm{C}}}{\Lambda^4}\,. \tag{5}$$

Here, the F_{I} parameter belongs to the interference between the contact interaction and the SM, while the F_{C} parameter represents only the contact interaction. These parameters do not depend on the compositeness scale and are a function of cross section. At high-Λ values, the second term in Eq. (5) dominates in contribution to the total cross section. Therefore, the interference of the four-fermion contact interaction with the SM could be accepted as the leading term in our calculations.

3. Method and analysis

In this study, the contact interaction scales that the *ep* collider mentioned in the introduction could reach in various interaction scenarios are estimated for different statistical significances. To investigate the sensitivity of new contact interactions, particle final-state distributions were used. These distributions are the transverse momentum (p_{t}) and pseudo-rapidity (η) distributions of electrons and jets. These distributions were obtained separately for the contact interaction models with various compositeness scales and SM using the CalcHEP program. As an example, the distributions regarding the $\Lambda_{\rm LL}^{+}$ model are shown in Figs. 1 and 2. The production of the desired distributions using the cross-section values obtained from the CalcHEP program was achieved with the ROOT program [24]. CT10 parton distribution function (PDF) was used in the CalcHEP program [25]. Later, different PDFs were used to see the changes in the scaling results.

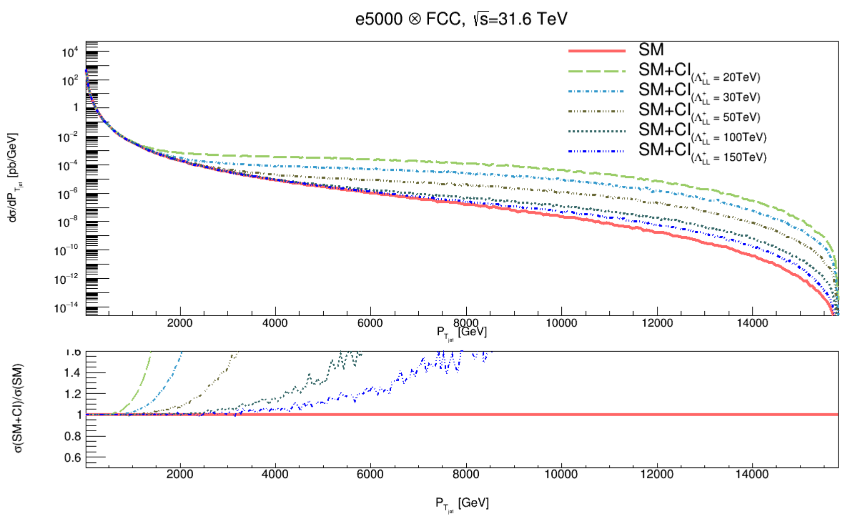

Fig. 1. Transverse momentum distribution for jet final states and the model of $\Lambda_{\rm LL}^{+}$.

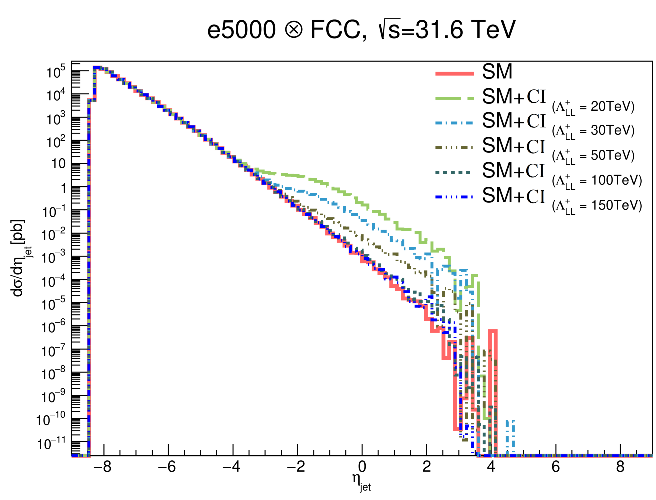

Fig. 2. Pseudo-rapidity distribution for jet final states and the model of $\Lambda_{\rm LL}^{+}$.

Our aim was to determine the kinematic cuts by comparing the distributions of the contact interaction model with those of the SM. The calculated cut values are given in Table 1. In this table, the p_{t} cut is given as the minimum value, and in the remaining part of the analysis, sensitivity calculations were made by increasing these cut values at different rates. In sensitivity calculations, η cuts were used without modification as stated in Table 1. The cut value for η_{electron} was taken as $|\eta| < 2.5$ for all interaction scenarios, taking into account the detector acceptability and geometry. In the CMS experiment, electromagnetic and hadron calorimeters are placed in the field with $|\eta| < 3$. Outside the field, hadron calorimetry is located with $3 < |\eta| < 5$ [26].

Table 1. The cut values determined by comparing of the distributions of the particle final states in terms of SM and SM+CI.

Model	$p_{\mathrm{t}}(e, \mathrm{jet})$ [GeV]	η_{jet}	η_{electron}
$\Lambda_{\mathrm{LL}}^{+}$	> 600	$-4 < \eta < 1$	$\|\eta\| < 2.5$
$\Lambda_{\mathrm{LL}}^{-}$	> 600	$-4.5 < \eta < 1$	$\|\eta\| < 2.5$
$\Lambda_{\mathrm{LR}}^{+}$	> 400	$-4.8 < \eta < 1$	$\|\eta\| < 2.5$
$\Lambda_{\mathrm{LR}}^{-}$	> 800	$-4 < \eta < 1$	$\|\eta\| < 2.5$
$\Lambda_{\mathrm{RL}}^{+}$	> 400	$-4.5 < \eta < 1$	$\|\eta\| < 2.5$
$\Lambda_{\mathrm{RL}}^{-}$	> 500	$-4.5 < \eta < 1$	$\|\eta\| < 2.5$
$\Lambda_{\mathrm{RR}}^{+}$	> 400	$-4.6 < \eta < 0.5$	$\|\eta\| < 2.5$
$\Lambda_{\mathrm{RR}}^{-}$	> 700	$-4 < \eta < 1$	$\|\eta\| < 2.5$

In this study, the statistical significance calculation was made as given in Eq. (6)

$$\sigma_{\mathrm{s}} = \frac{\sigma_{\mathrm{SM+CI}} - \sigma_{\mathrm{SM}}}{\sqrt{\sigma_{\mathrm{SM}}}} \times \sqrt{\mathcal{L}}\,. \tag{6}$$

Here, $\sigma_{\mathrm{SM+CI}}$ represents the signal cross section estimated based on the contact interaction model, and σ_{SM} represents the background cross section based only on SM. Here, $\mathcal{L}$ is the integrated luminosity value. The calculations aimed to determine the contact interaction scales that lead to statistical significance values (σ_{s}) of 2, 3, and 5. These significance values represent the following sensitivities: 2, 3, and 5 σ_{s} and they could be considered as the sign of a New Physics, a new observation, and limit values for a discovery, respectively. In the next stage of the analysis, the cuts specified in Table 1 were applied and the signal cross sections along with the SM cross sections were determined for contact interaction models with different scales. We can call this process Λ scanning. In the Λ scan, the corresponding signal cross sections were determined by changing the Λ values with very small intervals.

In the rest of the analysis, Eq. (6) was evaluated with different luminosity values, and the cross sections leading to the specified $\sigma_{\rm s}$ values and the corresponding Λ values were found. This analysis, that is, the determination of Λ values, was carried out by the following method: for a certain luminosity value, the distribution of the $\sigma_{\rm s}$ values corresponding to each Λ was fitted with an appropriate function (higher-order polynomial), and the Λ values regarding the desired $\sigma_{\rm s}$ were determined using this function.

4. Results

In this section, first of all, we present the results obtained with an integrated luminosity of 10 fb^{-1} for 5 TeV $\otimes$ 50 TeVep option. The numbers of signal events that will lead to different statistical significance are presented in Fig. 3 depending on the $p_{\rm t}$ cuts. This is intended to give an idea about the effect of the cuts on the number of events. The event numbers were obtained by multiplying the cross-section values and the integrated luminosities. When we look at Fig. 3, we can clearly see the following: when the $p_{\rm t}$ cut is increased from 2000 GeV, there is a sharp decrease in the number of signal events. While the number of signal events decreases to 119 for 5σ at the $p_{\rm t} > 4000$ GeV cut, this value becomes 55 at the $p_{\rm t} > 5000$ GeV cut. On the other hand, this number was found to be 1036 in the $p_{\rm t} > 2000$ GeV cut.

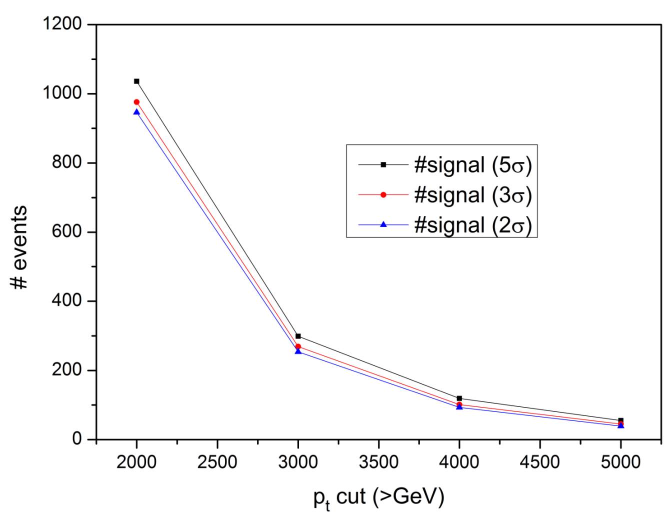

Fig. 3. The numbers of signal events that lead to different statistical significances are shown based on $p_{\rm t}$ cuts.

In this part of the manuscript, the contact interaction scale values that will lead to different statistical significances (5σ, 3σ, and 2σ) are shown in Figs. 4, 5, and 6 for different models depending on the p_{t} cuts. These three graphs together could be said to have the following trends: It could be seen that the highest-Λ values can be achieved by far with the $\Lambda_{\mathrm{LL}}^{+}$ and $\Lambda_{\mathrm{RR}}^{+}$ models. The lowest Λ values are reached by $\Lambda_{\mathrm{LR}}^{-}$, and $\Lambda_{\mathrm{RL}}^{-}$ models. An increasing trend in scale values with the p_{t} cut is observed in all models.

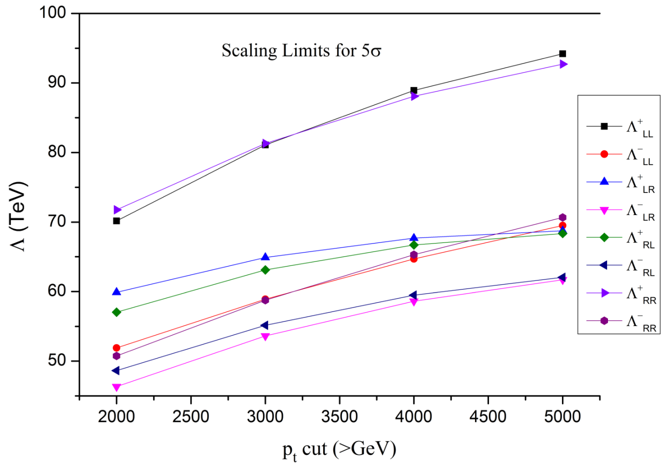

Fig. 4. Contact interaction scales are shown for 5σ and different models according to different p_{t} cuts.

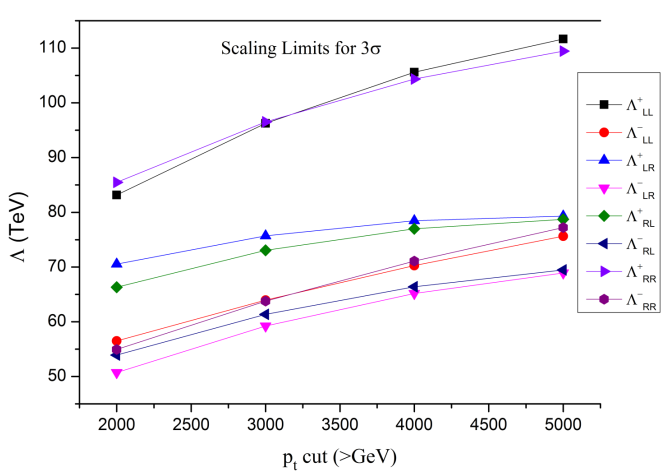

Fig. 5. Contact interaction scales are shown for 3σ and different models according to different p_{t} cuts.

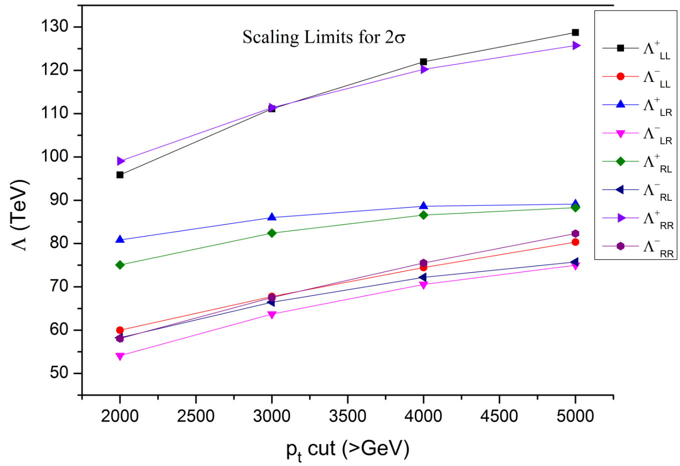

Fig. 6. Contact interaction scales are shown for 2σ and different models according to different $p_{\rm t}$ cuts.

Two different cuts were taken into consideration to see the rate of change in the scale ($p_{\rm t} > 2000; p_{\rm t} > 4000$). The change in scale with the $p_{\rm t}$ cut is presented as a percentage for different models in Fig. 7. According to this graph, the change is generally over 20% and at most 30%, but it is at lower levels for two models. It is 9% *versus* 15% for $\Lambda^+_{\rm LR}$ and $\Lambda^+_{\rm RL}$, respectively, regarding 2σ. Finally, the limit values for contact interaction scales are

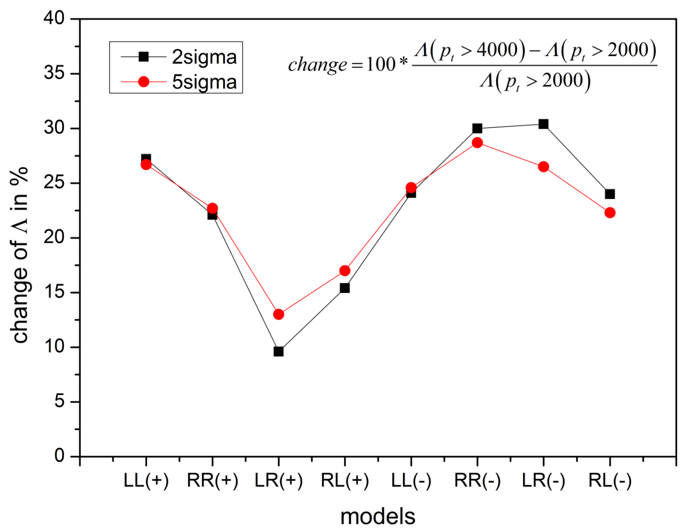

Fig. 7. The change of Λ with $p_{\rm t}$ cut in % for 2σ and 5σ in terms of interaction models.

given in summary with two graphs of Figs. 8 and 9 for two different p_t cuts ($p_t > 2000; p_t > 4000$). Looking at these two graphs, the following evaluations could be made: When the models for destructive interferences are compared, it is seen that similar values are obtained. For constructive

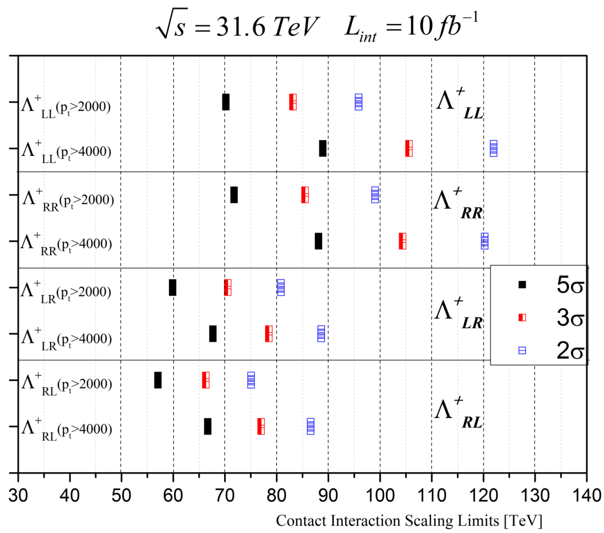

Fig. 8. Contact interaction scales are shown for the specified models with two different p_t cuts and different sensitivities.

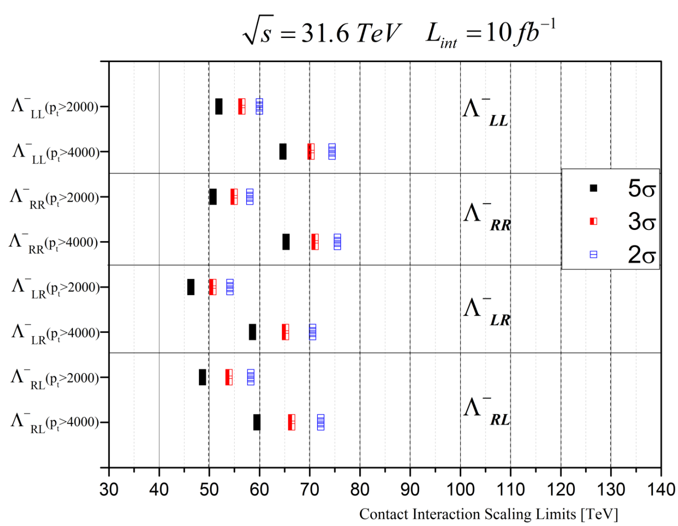

Fig. 9. Contact interaction scales are shown for the specified models with two different p_t cuts and different sensitivities.

interferences, close values are seen in two groups. It could be said that close values were obtained for Λ^+_{LL} and Λ^+_{RR} in the first group and for Λ^+_{LR} and Λ^+_{RL} in the other group. Thus, changes in the scale are presented to the reader for evaluation depending on p_{t} cuts, models, and sensitivities. It should also be noted that all these results were obtained by cut-based analysis.

At this level of study, several uncertainties that could affect our results were evaluated as follows: uncertainty that may occur with different selection of QCD scaling, changes in our results as a result of different PDF selection, the effect of uncertainty in the luminosity, uncertainty in electron reconstruction efficiency, and uncertainty in p_{t} resolution. All uncertainties were calculated based on a 2σ statistical significance level. First, the effect of changes in luminosity was determined. For this purpose, the luminosity value of 10 fb^{-1} was changed by increasing and decreasing it from 1% to 5% in Eq. (6) and the scaling limits were recalculated. The results are shown as percentage changes in Fig. 10. The results show the largest change and

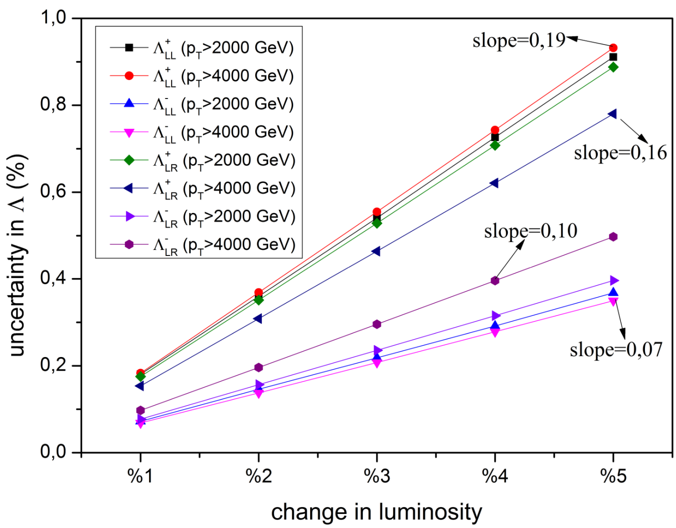

Fig. 10. Percentage uncertainty in Λ for 2σ in terms of changes in luminosity.

its absolute value if negative. The figure shows the difference between the results obtained with positive and negative models. It can be said that this is due to the fact that the distribution of scaling values depending on the significance values is in a different form for positive and negative models (Figs. 11 and 12). It is also seen that the uncertainty in the scaling is at most around 0.93% for a 5% change in luminosity. The results do not change significantly with the p_{t} cu-toff.

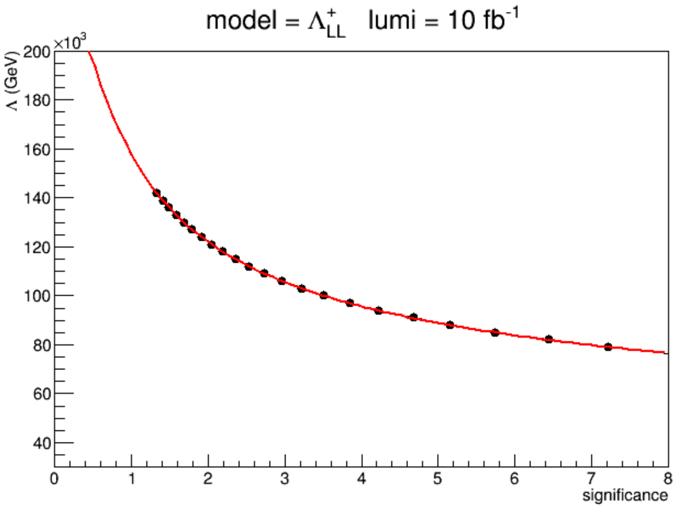

Fig. 11. Distribution of Λ (black dots) depending on the significance values in the constructive interference of the $\Lambda_{\rm LL}$ model and the fit function (red line) ($p_{\rm t} >$ 4000 GeV).

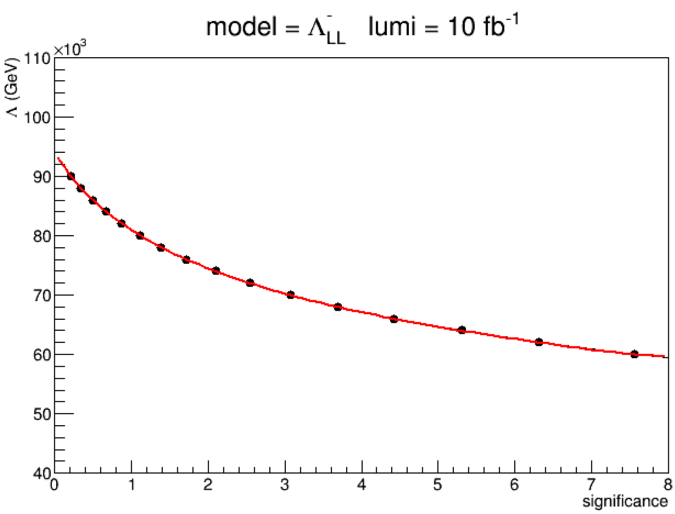

Fig. 12. Distribution of Λ (black dots) depending on the significance values in the destructive interference of the $\Lambda_{\rm LL}$ model and the fit function (red line) ($p_{\rm t} >$ 4000 GeV).

The default value for QCD scaling in CalcHEP is the invariant mass of the incoming particles, the electron and proton in the present case, $M_{ep} = \sqrt{(p_e + p_p)^2}$. The scaling limits were recalculated by taking twice ($2 \times M_{ep}$) and half ($0.5 \times M_{ep}$) of this value for both CI and SM. Differences from the default value are shown as percentage changes in Fig. 13. Here too, the difference between the results obtained with the positive and negative models is evident. It is seen that the uncertainty in Λ does not exceed 1% and 0.6% for positive and negative models, respectively. Moreover, it can be said that the results do not change significantly with the $p_{\rm t}$ cut-off. The results show the largest change and its absolute value if negative.

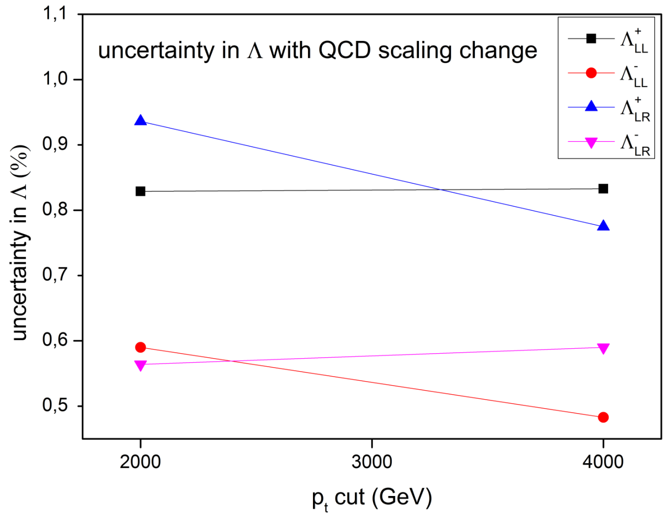

Fig. 13. Uncertainties obtained for Λ by taking twice and half of the default value in QCD scaling.

Another uncertainty may arise from the use of different PDFs. For this reason, the calculations were repeated using 5 different PDFs other than CT10 in CalcHEP for both CI and SM. PDFs used are: mrst2004, nnpdf230130, nnpdf310118, nnpdf310130, pdf4LHC15. Percentage changes compared to the results obtained with CT10 are shown in Fig. 14 for $p_{\rm t} > 2000$ GeV. The first thing that stands out here is that the uncertainties obtained for the $\Lambda^+_{\rm LR}$ and $\Lambda^-_{\rm LR}$ models are quite low compared to the other models and are at most 1.6%. On the other hand, it is seen that this uncertainty exceeds 4% and 5% levels for some distribution functions in $\Lambda^+_{\rm LL}$ and $\Lambda^-_{\rm LL}$, respectively. In addition, PDFs that cause high uncertainty differ according to the models.

The uncertainty in electron reconstruction and ID efficiency is reported as 2% for $p_{\rm t} > 200$ GeV [27]. The uncertainty calculation was made assuming that this would affect the cross section of interest at the same rate. The

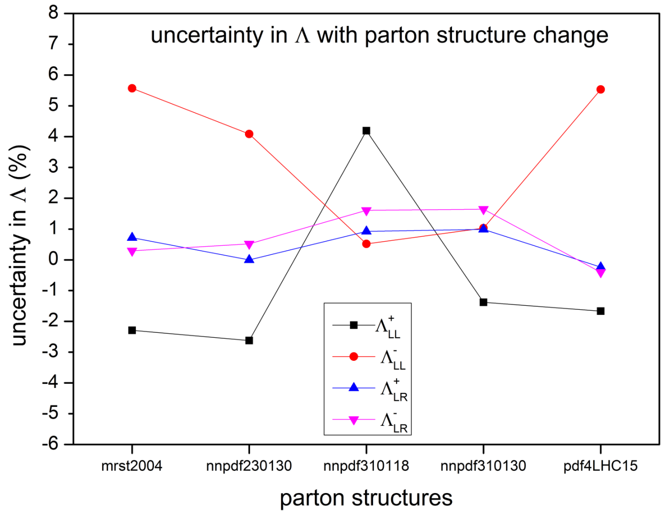

Fig. 14. Uncertainties obtained for Λ using different PDFs ($p_{\mathrm{t}} > 2000$ GeV).

calculations were re-performed by conservatively taking the reconstruction efficiency as 90%, and increasing and decreasing the cross sections by 0.2% only for CI. The results in Fig. 15 show the largest change and its absolute value if negative. The uncertainty in Λ was at least 0.21% and at most 1.16% in the negative LR and positive LL model, respectively.

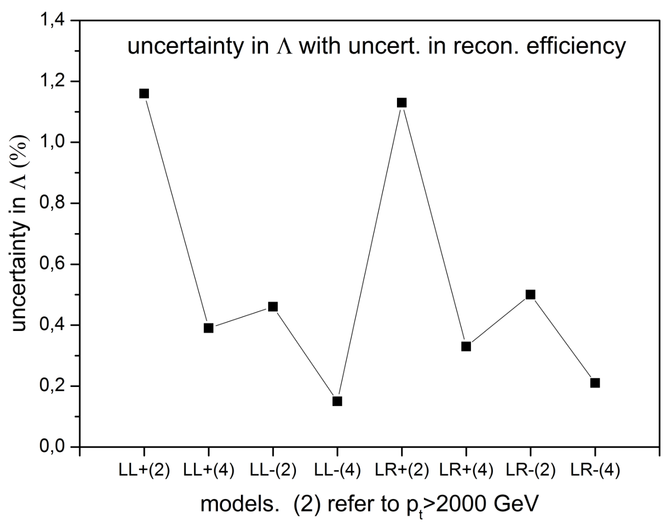

Fig. 15. Uncertainties in Λ arising from uncertainty in e reconstruction efficiency.

Jet p_{t} resolution was included in our uncertainty calculation as follows: calculations were repeated assuming that the resolution at high p_{t} was 0.5% and an uncertainty at this resolution of 10%. For this, the calculations were repeated for $p_{\mathrm{t}} > 2000$ GeV by taking $p_{\mathrm{t}} > 1990$ GeV and $p_{\mathrm{t}} > 2010$ GeV. Then $p_{\mathrm{t}} > 4000$ GeV, $p_{\mathrm{t}} > 3980$ GeV and $p_{\mathrm{t}} > 4020$ GeV were taken. These new calculations were made only for CI. Our anlaysing method was found to be significantly sensitive to this uncertainty, and significant differences occurred between models. The uncertainty in Λ was at least 1.20% and at most 10.38% in the negative LL($p_{\mathrm{t}} > 4000$ GeV) and positive LL($p_{\mathrm{t}} > 2000$ GeV) model, respectively. It has been observed that decreasing the p_{t} cut-off gives greater changes than increasing it. The results in Fig. 16 show the largest changes. It can also be seen that the uncertainty decreases significantly with the increase in the p_{t} cut-off. It is also clear that when the uncertainty in the resolution is taken lower, the uncertainty in the Λ will be significantly less.

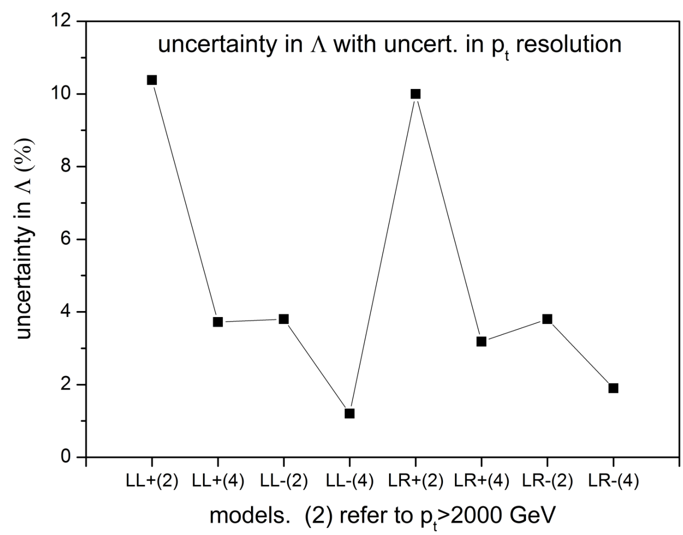

Fig. 16. Uncertainties in Λ arising from 10% uncertainty in p_{t} resolution.

In our study, the statistical uncertainty calculation was made as follows: when each significance calculation is made according to Eq. (6) for a given model and interaction scenario, a statistical error is determined depending on the correlation factor (ρ) according to the standard error propagation. This error value was multiplied by a uniformly distributed random number between -1 and $+1$ and added to the significance value. Scaling limit calculations were repeated with the newly obtained significance values. This was repeated 10 000 times to obtain the distribution of percentage differences from the default value. The sum of the mean and r.m.s. values of this distribution is presented as the statistical error in Fig. 17. Six different correlation factors were used in these calculations: 0.0, 0.50, 0.70, 0.90, 0.95, and 0.99. As can be seen, when the factor 0.99 is used, the error is quite low. When the

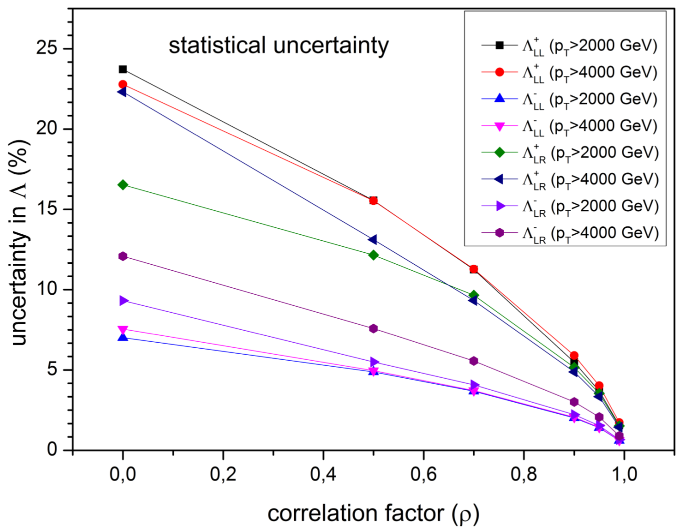

Fig. 17. Statistical uncertainties in Λ for different correlation factors.

factor is taken as 0.0, significant errors occur. The difference between positive and negative models is particularly evident at low correlation factors. It could be said that reasonable error rates can be obtained at relatively high correlation factors. An attempt was made to obtain information about the correlation factor. For this purpose, the electromagnetic (EE) and contact interaction (gci) coupling constants were fluctuated to make the cross sections compatible with the statistical uncertainty and the calculations were repeated. Here, exactly the same electromagnetic coupling constants were used for the signal and background. Accordingly, 1000 events were simulated and the correlation factor was determined as 1.00 ± 0.04 with Eq. (7) (see Fig. 18)

$$\begin{aligned}
\mathrm{Corr}\left\{x,y\right\} &= \frac{\mathrm{Cov}\left\{x,y\right\}}{\sqrt{\mathrm{Var}\left\{x\right\}\mathrm{Var}\left\{y\right\}}}\,, \\
\mathrm{Var}\left\{x\right\} &= E\left\{\left(x-E\left\{x\right\}\right)^2\right\}\,, \\
\mathrm{Cov}\left(x,y\right) &= E\left\{\left(x-E\left\{x\right\}\right)\left(y-E\left\{y\right\}\right)\right\}\,. \qquad (7)
\end{aligned}$$

Here, x and y represent signal and background, respectively. $E\left(x\right)$ refers to the expected value of x.

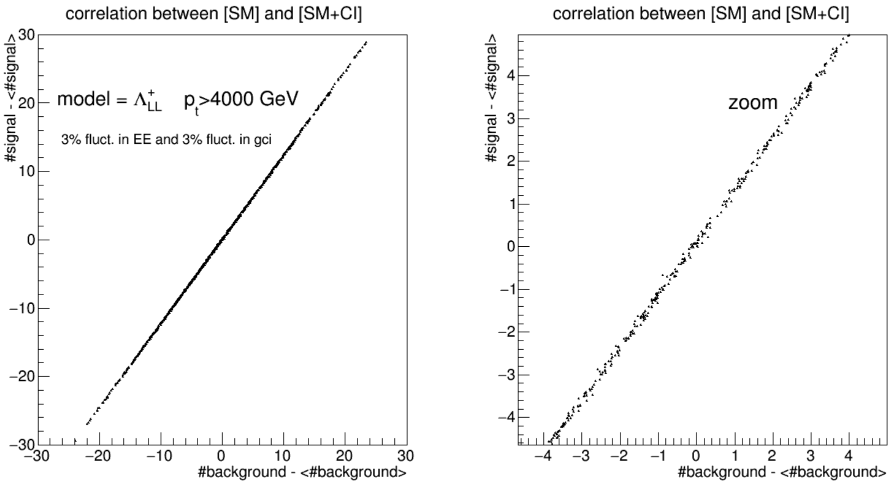

Fig. 18. Correlation between signal and background. EE refers to electromagnetic coupling constant and gci refers to the contact interaction coupling constant. The signal and background have the same EE constants in fluctations.

Finally, the effects of possible systematic changes in cross-section values were determined. For this purpose, scaling limits were recalculated by increasing or decreasing the cross sections from 1% to 10% for a given model and for both CI and SM simultaneously. Percentage changes in the scaling limits compared to the initial state are shown in Fig. 19. Under the same

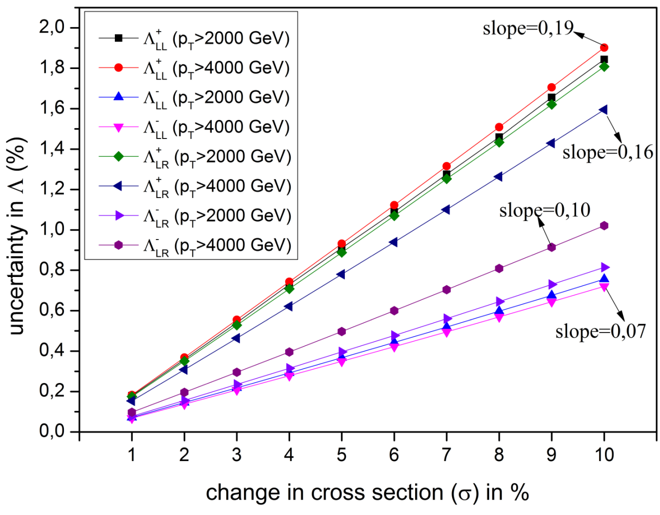

Fig. 19. Uncertainties in Λ arising from changing the cross sections at different rates.

conditions, reducing the cross sections gives larger changes than increasing them. The absolute value of the changes is given in the figure. Here too, the difference between the results of the positive and negative models is evident and appears in two separate groups. It could be seen that the results regarding $\Lambda^+_{\mathrm{LR}}(p_{\mathrm{t}} > 4000$ GeV) and $\Lambda^-_{\mathrm{LR}}(p_{\mathrm{t}} > 4000$ GeV) models are somewhat separated from their groups. According to the results, the uncertainty in Λ was highest in the positive model as 0.93% and 1.90% at 5% and 10% changes in the cross sections, respectively. On the other hand, for 5% and 10% changes in cross sections, the uncertainty in Λ was at least 0.35% and 0.72% in the negative model, respectively.

All these uncertainties are summarized in Tables 2 and 3. The results are given for the 3% change in luminosity, 10% uncertainty in p_{t} resolution, 0.95 as correlation factor (ρ), and 10% change in cross sections. The total uncertainties are calculated as the quadratic sum of the individual uncertainties. In the table, two different total uncertainty values were calculated by taking the maximum and average uncertainty values originating from the PDF. As can be seen from the table, the largest contribution to the total uncertainty comes from PDF change, uncertainty in p_{t} resolution, and statistical uncertainty. It could be said that other uncertainty sources have a relatively low impact.

Table 2. The uncertainties in Λ for a different kind of sources. Total uncertainties are the quadratic summation of individual ones. $\Delta\Lambda(2)$ and $\Delta\Lambda(4)$ refer to $\Delta\Lambda\,(p_{\mathrm{t}} > 2000\,GeV)$ and $\Delta\Lambda(p_{\mathrm{t}} > 4000$ GeV), respectively. Uncertainty in Λ for different sources in %.

Error source	$\Delta\Lambda^+_{\mathrm{LL}}(2)$	$\Delta\Lambda^+_{\mathrm{LL}}(4)$	$\Delta\Lambda^-_{\mathrm{LL}}(2)$	$\Delta\Lambda^-_{\mathrm{LL}}(4)$
Luminosity 3%	0.54	0.56	0.22	0.21
QCD scale	0.83	0.83	0.59	0.48
Uncert. recon. eff.	1.16	0.39	0.46	0.15
Uncert. p_{t} resol. 10%	10.38	3.72	3.80	1.22
Stat. uncert. $\rho = 0.95$	3.69	4.02	1.41	1.43
Cross section 10%	1.84	1.90	0.76	0.72
Parton — maximum	4.19	2.66	5.57	3.16
Parton — average	2.43	1.30	3.35	1.56
Total % — parton max.	12.03	6.47	6.97	3.78
Total % — parton avg.	11.53	6.04	5.37	2.60

Table 3. The uncertainties in Λ for a different kind of sources. Total uncertainties are the quadratic summation of individual ones. $\Delta\Lambda(2)$ and $\Delta\Lambda(4)$ refer to $\Delta\Lambda(p_{\mathrm{t}} > 2000$ GeV) and $\Delta\Lambda(p_{\mathrm{t}} > 4000$ GeV), respectively. Uncertainty in Λ for different sources in %.

Error source	$\Delta\Lambda^{+}_{\mathrm{LR}}(2)$	$\Delta\Lambda^{+}_{\mathrm{LR}}(4)$	$\Delta\Lambda^{-}_{\mathrm{LR}}(2)$	$\Delta\Lambda^{-}_{\mathrm{LR}}(4)$
Luminosity 3%	0.53	0.46	0.24	0.30
QCD scale	0.94	0.78	0.56	0.59
Uncert. recon. eff.	1.13	0.33	0.50	0.21
Uncert. p_{t} resol. 10%	10.00	3.18	3.80	1.90
Stat. uncert. $\rho = 0.95$	3.54	3.34	1.54	2.08
Cross section 10%	1.81	1.60	0.81	1.02
Parton — maximum	0.99	1.65	1.65	2.04
Parton — average	0.58	0.74	0.90	1.01
Total % — parton max.	10.92	5.24	4.56	3.69
Total % — parton avg.	10.89	5.03	4.35	3.24

After this point, the second option, 50 GeV $\otimes$ 50 TeVep, was considered. In the first stage of this analysis, the cut-based procedure analogous to the first option was considered. The different η_{jet} and p_{t} cuts were evaluated for different interaction models and the best results obtained are summarized in Fig. 20 for the luminosity of 190 fb^{-1}. The uncertainties are shown in Table 4. Also, the development of the scaling limits corresponding to luminosities between 10 fb^{-1} to 190 fb^{-1} were determined. They are shown for two different models in Figs. 21 and 22. It is seen that if the η cut changes from $\eta_{\mathrm{jet}} > -5$ to $\eta_{\mathrm{jet}} > -6$, a significant improvement in the contact interaction scale is achieved ($\Lambda^{+}_{\mathrm{LL}} = 30.8$ TeV for 2σ). Although there is no detector acceptability reference for this cut-off, the results are presented because they demonstrate a significant increase in scaling limits.

Especially when the results in the $\Lambda^{-}_{\mathrm{LL}}$ model were evaluated, it was seen that the bin-by-bin analysis should be done. For this analysis, $\Lambda^{+}_{\mathrm{LL}}$ and $\Lambda^{-}_{\mathrm{LL}}$ models with $-5 < \eta_{\mathrm{jet}} < 0.5$ cut were used. To this end, $p_{\mathrm{t,jet}}$s were divided into 25 bins between 200 GeV and 1580 GeV. This upper limit was set because no cross-section values greater than 0 were obtained after 1580 GeV. The bins were arranged such that the bin resolution was not greater than the bin width, according to Eq. (8) [15]. The criterion used to determine Λ was $\chi^2/\mathrm{n.d.f.} \approx 1.20$ (standard criteria to set lower limits on Λ) by taking into account the signal and background number of events with given luminosity. This analysis was performed for two different luminosities

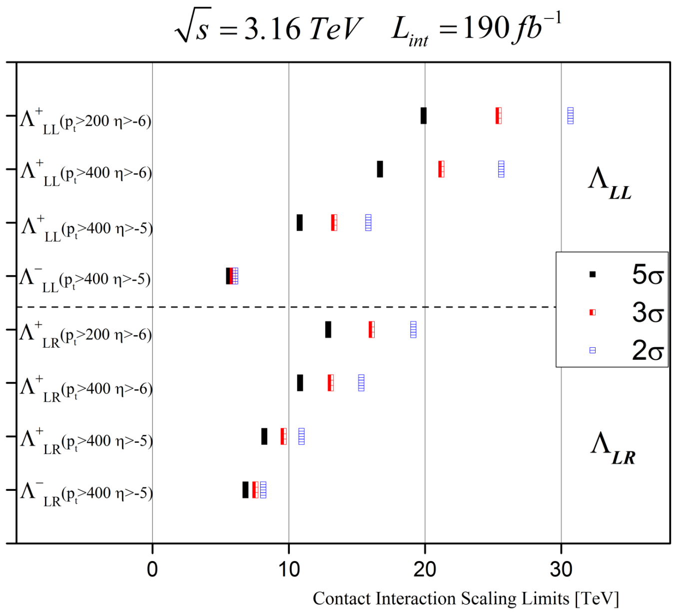

Fig. 20. Contact interaction scales are shown for the specified models with different kinematical cuts and sensitivities. The collider option is 50 GeV $\otimes$ 50 TeV*ep*.

Table 4. The uncertainties in Λ for different kind of sources. Total uncertainties are the quadratic summation of individual ones. $\Delta\Lambda\,(2)$ and $\Delta\Lambda\,(4)$ refer to $\Delta\Lambda\,(p_{\mathrm{t}} > 200$ GeV) and $\Delta\Lambda\,(p_{\mathrm{t}} > 400$ GeV), respectively. E6 and E5 refer to $-6 < \eta < 0.5$ and $-5 < \eta < 0.5$, respectively. Uncertainty in Λ for different sources in % (50 GeV $\otimes$ 50 TeV*ep*).

Error source	$\Delta\Lambda^+_{\mathrm{LL}}(2)$ E6	$\Delta\Lambda^+_{\mathrm{LL}}(4)$ E6	$\Delta\Lambda^+_{\mathrm{LL}}(4)$ E5	$\Delta\Lambda^-_{\mathrm{LL}}(4)$ E5
Luminosity 3%	1.40	1.42	1.27	0.23
Uncert. recon. eff.	10.23	2.73	0.25	0.07
Uncert. p_{t} resol. 10%	10.31	4.00	0.66	0.19
Stat. uncert. $\rho = 0.95$	4.70	4.92	4.93	1.39
Cross section 10%	2.41	2.44	0.64	0.41
Parton — average	6.00	3.91	5.24	4.00
Total %	16.64	8.42	7.37	4.27

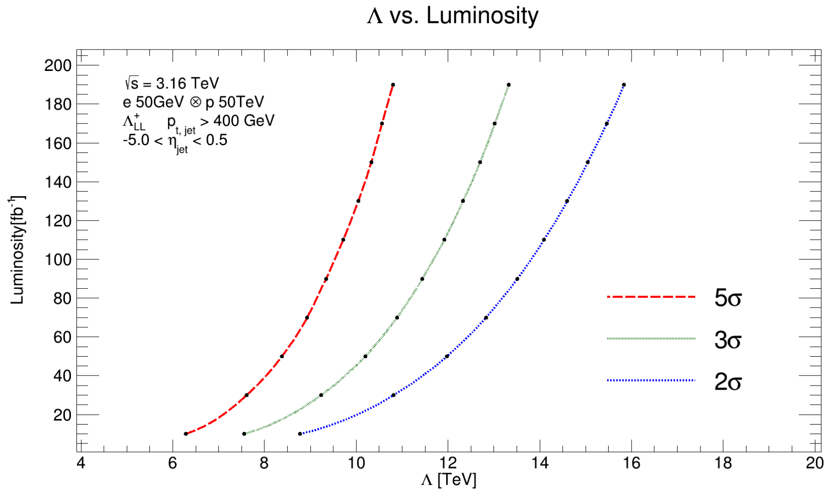

Fig. 21. Contact interaction scales for $\Lambda^{+}_{\mathrm{LL}}$ changing with luminosity. The collider option is 50 GeV ⊗ 50 TeV*ep*.

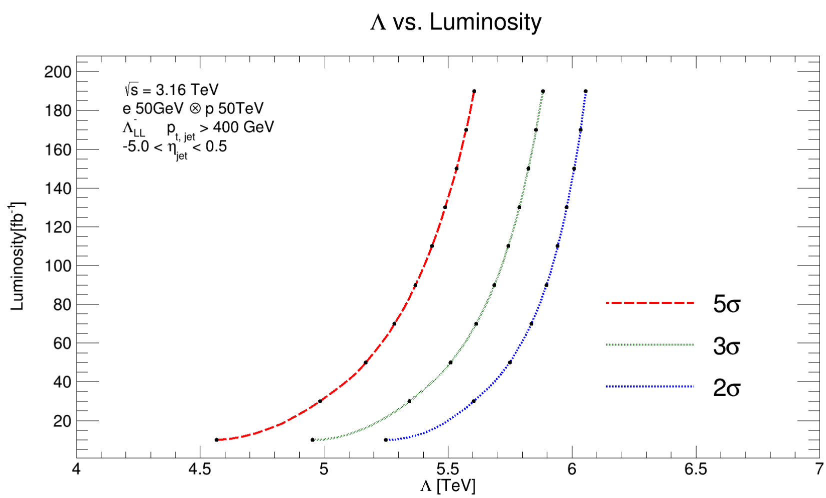

Fig. 22. Contact interaction scales for $\Lambda^{-}_{\mathrm{LL}}$ changing with luminosity. The collider option is 50 GeV ⊗ 50 TeV*ep*.

of 190 fb^{-1} and 300 fb^{-1}. The results are shown in Table 5. Only statistical error was included in the results. For this, the statistical error was calculated on χ^2/n.d.f. by taking $\rho = 0.99$ and the Λ value corresponding to this uncertainty was determined. As an example, the distribution of signal ($\Lambda^{-}_{\mathrm{LL}} = 12.6$ TeV) and background event numbers by bins is shown in Fig. 23. When the results are examined, it is seen that there is an improvement in

Table 5. Λ obtained with bin-by-bin analysis according to χ^2/n.d.f. It is compared to the cut-based analysis with 2σ significance. Λ with bin-by-bin analysis for two different luminosities. Errors for bin analysis are statistical ($-5.0 < \eta_{\rm jet} < 0.5$) 50 GeV $\otimes$ 50 TeV*ep*.

Model	Luminosity [fb^{-1}]	χ^2/n.d.f.	Λ [TeV] with bin analysis	Λ [TeV] with cut-based analysis
$\Lambda^+_{\rm LL}$	190	1.21	14.5 ± 1.0	15.84 ± 1.17
$\Lambda^+_{\rm LL}$	300	1.20	16.0 ± 1.0	17.6 ± 1.3
$\Lambda^+_{\rm LL}$	600	1.19	18.0 ± 1.0	20.4 ± 1.51
$\Lambda^-_{\rm LL}$	190	1.20	10.0 ± 1.3	6.06 ± 0.26
$\Lambda^-_{\rm LL}$	300	1.22	12.6 ± 1.2	—
$\Lambda^-_{\rm LL}$	600	1.21	16.0 ± 1.0	—

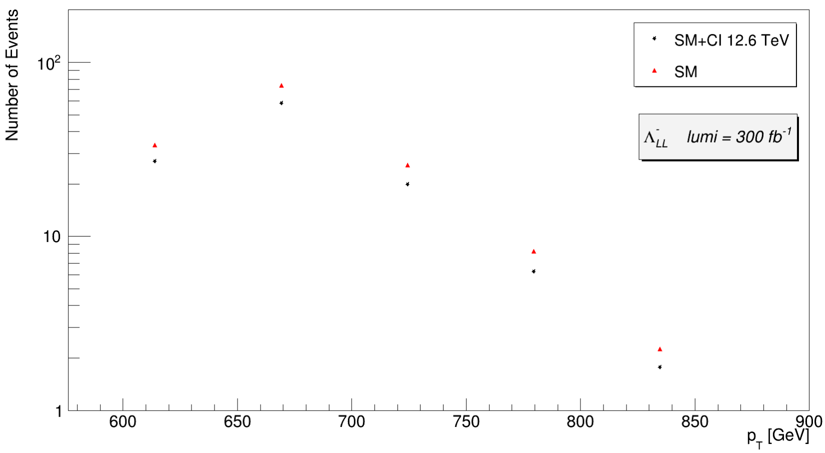

Fig. 23. Number of events by bins for signal ($\Lambda^-_{\rm LL} = 12.6$ TeV) and background. This distribution leads to χ^2/n.d.f. $= 1.22$. The collider option is 50 GeV $\otimes$ 50 TeV*ep*.

the $\Lambda^-_{\rm LL}$ model compared to the cut-based analysis

$$\begin{aligned} \sigma_{p_{\rm t}} &= p_{\rm t}\sqrt{-\frac{n^2}{p_{\rm t}^2} + \frac{s^2 p_{\rm t}^m}{p_{\rm t}} + c^2}\,, \\ n &= 5.09\,, \qquad s = 0.512\,, \qquad m = 0.325\,, \qquad c = 0.033\,. \end{aligned} \tag{8}$$

In this part of the manuscript, the evaluation of the results presented in this study will be done with different collider options. It is clear that very high-Λ values are obtained in the analysis performed with the 5 TeV $\otimes$ 50 TeVep option. These collider parameters can be considered as a hypotetical option. This option has been studied considering the development of the relevant accelerator technology. In addition, it is aimed to provide comparison with different accelerator options. The results received at high luminosity with the 50 GeV $\otimes$ 50 TeVep option could be considered comparable to those obtained in previous higher-energy LHC pp collisions [14, 15, 28–30]. Besides, it was shown that significant improvement could be achieved with changing kinematic cuts essentially for pseudo-rapidity. On the other hand, considering these results, it does not seem possible for the 50 GeV$\otimes$50 TeVep option to compete with the proposed FCC-hh 100 TeV option [31, 32], which is the main focus of the FCC and has much higher energy than LHC.

Several studies have been conducted on the feasibility, future prospects, and physics potential of the muon–hadron collider [33–41]. The advantages of the μp collider over an ep or pp collider could be mentioned. The difficulty in reaching high energies due to the synchrotron radiation in the ep colliders is much less in the μp collider. Also, μp colliders have less QCD background than pp colliders. A phenomenological study based on the FCC-μp collider has been carried out at several muon energies $(0.75, 1.5, 3, 20$ TeV$)$ [42]. The results are compared with those presented in this manuscript. It is seen that the results obtained with the option of 3 TeV $\otimes$ 50 TeVμp give very close results to those with the 5 TeV $\otimes$ 50 TeVep option with some luminosity arrangements. Besides, it is seen that with 20 TeV $\otimes$ 50 TeVμp, very high-Λ limits could be achieved. It could also be said that the results obtained with the 50 GeV $\otimes$ 50 TeVep option do not come very close to those with any μp collider option mentioned above. It should also be noted that the energy difference is large with the 50 GeV $\otimes$ 50 TeVep option compared to the proposed μp option.

After all these comparisons, the high-luminosity 125 GeV $\otimes$ 50 TeVep option was considered by taking account of the proposed linear collider with energy recovery (ERLC) using superconducting technology [43]. This option has been studied for two different η cuts and a wide range of luminosity values with bin-by-bin analysis. The results are shown in Table 6. In the selection of bins, it was ensured that the momentum resolution did not exceed the bin width. Also, bins with an event number below 10 were not included in the calculation. Moreover, bins belonging to the high-p_{t} region where cross-section fluctuations are large were not included.

Significant improvement is seen compared to the 50 GeV $\otimes$ 50 TeVep option. For example, it is seen that the 62 TeV Λ limit value could be achieved with the $\Lambda^{+}_{\mathrm{LL}}$ model. Based on these results, it could be said that the high-luminosity 125 GeV$\otimes$50 TeVep option may compete with the option of 750 GeV $\otimes$ 50 TeVμp and 1500 GeV $\otimes$ 50 TeVμp at low luminosity.

Table 6. Λ obtained with bin-by-bin analysis according to χ^2/n.d.f. Λ with bin-by-bin analysis for different luminosities. Errors for bin analysis are statistical 125 GeV $\otimes$ 50 TeVep.

Luminosity $[\mathrm{fb}^{-1}]$	Model	Λ [TeV] $-5.0 < \eta_{\mathrm{jet}} < 0.5$	Λ [TeV] $-5.6 < \eta_{\mathrm{jet}} < 0.5$
300	Λ^+_{LL}	41.5 ± 2.0	45.0 ± 2.5
300	Λ^-_{LL}	38.5 ± 2.5	43.0 ± 2.5
600	Λ^+_{LL}	49.0 ± 2.5	53.0 ± 3.0
600	Λ^-_{LL}	46.0 ± 2.5	51.0 ± 1.7
900	Λ^+_{LL}	54.0 ± 2.5	58.0 ± 2.0
900	Λ^-_{LL}	51.0 ± 2.0	56.0 ± 3.0
1200	Λ^+_{LL}	57.0 ± 2.0	62.0 ± 2.0
1200	Λ^-_{LL}	55.0 ± 2.0	60.0 ± 3.0

5. Conclusion

The method in this study can be considered as determining the contact interaction scale limits for certain sensitivities by cut-based analysis. Additionally, the bin-by-bin analysis was performed for some interaction scenarios. By continuously increasing the transverse momentum cuts of the final jets at certain rates, the deviations of the contact interaction models from the SM were evaluated over the total cross sections. For each cut-off value, statistical significance values were obtained by the method we call Λ scanning, corresponding to the scales listed at certain intervals. Since the Λ scan is done for all models and each of their cuts together with uncertainty calculation, it could be said that this process of analysis is time-consuming and tiring. The aim of the graphs presented in the results section is to evaluate the sensitivities of the contact interaction models depending on different factors. The Λ values corresponding to different sensitivities are presented in summary to evaluate the differences between the models. All these results are presented for the evaluation of the reader. The analysis performed does not lead to the production of results independent of the selected data set. In this analysis, the results and the conditions that produce them are clearly stated. The changes in the results according to the conditions considered, in other words, to certain kinematic cuts and models, are observed together with the uncertainties taken into account.

Many uncertainty sources were examined according to two different p_{t} cuts with the cut-based analysis. It is clear that the scaling limits increase significantly with the increase in the cut-off value. When the results in Tables 2 and 3 are examined, it is seen that the total uncertainties decrease with the increase in the cut-off value. The differences in uncertainties according to positive and negative models were also observed. The sensitivity of the statistical uncertainty calculation to the correlation factor in the standard error propagation was determined. Our study is basically based on the cross sections obtained from CalcHEP. In order to determine the sensitivity of the scaling limits obtained for the cross sections, the calculations were repeated by changing CI and SM cross sections simultaneously at certain rates. The changes determined in the limits are presented as uncertainties.

Three collider options were studied: 5000 GeV $\otimes$ 50 TeVep, 50 GeV $\otimes$ 50 TeVep, and 125 GeV $\otimes$ 50 TeVep. The 5000 GeV $\otimes$ 50 TeVep option could be evaluated hypothetically, but it has been studied because it was considered an option that could be achieved with future accelerator technology. With this option, very high-Λ limits were determined and it was concluded that it could compete with the upcoming FCCμp collider. For the 50 GeV $\otimes$ 50 TeVep option which was initially a planned scenario in FCC, it was stated that this option with high luminosity could compete with LHCpp data and not with future higher-energy FCCpp and FCCμp. Finally, the 125 GeV $\otimes$ 50 TeVep option was studied with very high luminosity. It was concluded that this option could compete with higher-energy FCCμp at relatively low luminosity. In conclusion, it could be said that although the collider options studied in this manuscript do not demonstrate specific superiority over existing collider designs, it is thought that the presented study will contribute to a broader discussion of future collider possibilities.

I would like to thank Mehmet Şahin and Yusuf Oğuzhan Günaydın for their helpful discussions in this study.

REFERENCES

[1] J.I. Friedman, H.W. Kendall, «Deep inelastic electron scattering», *Annu. Rev. Nucl. Sci.* **22**, 203 (1972).

[2] A. Abada *et al.*, «FCC physics opportunities», *Eur. Phys. J. C* **79**, 474 (2019).

[3] S.I. Alekin *et al.*, «Prospects of the future ep-colliders», IHEP Preprint 87-48, 1987.

[4] U. Katz *et al.*, (eds.), «The THERA Book», DESY-LC-REV-2001-062, 2001.

[5] R. Brinkmann *et al.*, «Linac-Ring Type Colliders: Fourth Way to TeV Scale», arXiv:physics/9712023.

[6] A.N. Akay, H. Karadeniz, S. Sultansoy, «Review of linac-ring-type collider proposals», *Int. J. Mod. Phys. A* **25**, 4589 (2010).

[7] «Future circular collider study», 2024, https://fcc.web.cern.ch

[8] J.P. Delahaye *et al.*, «A beam driven plasma-wakefield linear collider from higgs factory to multi-tev», in: «Proceedings of the 5$^{\rm th}$ International Particle Accelerator Conference (IPAC)», *Dresden*, Germany 2014.

[9] A. Belyaev, N.D. Christensen, A. Pukhov, «Calchep 3.4 for collider physics within and beyond the standard model», *Comput. Phys. Commun.* **184**, 1729 (2013), arXiv:1207.6082 [hep-ph].

[10] A. Semenov, «LanHEP — A package for automatic generation of feynman rules from the Lagrangian. Version 3.2», *Comput. Phys. Commun.* **201**, 167 (2016), arXiv:1412.5016 [physics.comp-ph].

[11] ZEUS Collaboration (S. Chekanov *et al.*), «Search for contact interactions, large extra dimensions and finite quark radius in ep collision at HERA», *Phys. Lett. B* **591**, 23 (2004).

[12] H1 Collaboration (F. Aaron *et al.*), «Search for contact interactions in $e^{\pm}p$ collisions at HERA», *Phys. Lett. B* **705**, 52 (2011).

[13] ATLAS Collaboration (M. Aaboud *et al.*), «Search for new high-mass phenomena in the dilepton final state using 36 fb^{-1} of proton–proton collisions data at $\sqrt{s} = 13$ TeV with the ATLAS detector», *J. High Energy Phys.* **2017**, 182 (2017).

[14] CMS Collaboration (A.S. Sirunyan *et al.*), «Search for new physics in dijet angular distributions using proton–proton collisions at $\sqrt{s} = 13$ TeV and constraints on dark matter and other models», *Eur. Phys. J. C* **78**, 789 (2018).

[15] CMS Collaboration (S. Chatrchyan *et al.*), «Search for contact interactions using the inclusive jet p_{t} spectrum in pp collisions at $\sqrt{s} = 7$ TeV», *Phys. Rev. D* **87**, 052017 (2013).

[16] L3 Collaboration (M. Acciarri *et al.*), «Search for manifestations of new physics in fermion-pair production at LEP», *Phys. Lett. B* **489**, 81 (2000).

[17] OPAL Collaboration (G. Abbiendi *et al.*), «Tests of the standard model and constraints on new physics from measurements of fermion-pair production at 189–209 GeV at LEP», *Eur. Phys. J. C* **33**, 173 (2004).

[18] DELPHI Collaboration (J. Abdallah *et al.*), «Measurement and interpretation of fermion-pair production at LEP energies above the Z resonance», *Eur. Phys. J. C* **45**, 589 (2006).

[19] ALEPH Collaboration (S. Schael *et al.*), «Fermion pair production in e^+e^- collisions at 189–209 GeV and constraints on physics beyond the standard model», *Eur. Phys. J. C* **49**, 411 (2007).

[20] DELPHI Collaboration (J. Abdallah *et al.*), «A study of $b\bar{b}$ production in e^+e^- collisions at $\sqrt{s} = 130$–207 GeV», *Eur. Phys. J. C* **60**, 1 (2009).

[21] E.J. Eichten, K.D. Lane, M.E. Peskin, «New tests for quark and lepton substructure», *Phys. Rev. Lett.* **50**, 811 (1983).

[22] E.J. Eichten, I. Hinchliffe, K. Lane, C. Quigg, «Supercollider physics», *Phys. Rev. Lett.* **56**, 579 (1984); *Erratum ibid.* **58**, 1065 (1986).

[23] ATLAS Collaboration (G. Aad *et al.*), «Search for contact interactions and large extra dimensions in the dilepton channel using proton–proton collisions at $\sqrt{s} = 8$ TeV with the ATLAS detector», *Eur. Phys. J. C* **74**, 3134 (2014).

[24] R. Brun, F. Rademakers, «ROOT — An object oriented data analysis framework», *Nucl. Instrum. Methods Phys. Res. A* **389**, 81 (1997).

[25] H.L. Lai *et al.*, «New parton distributions for collider physics», *Phys. Rev. D* **82**, 074024 (2010).
[26] CMS Collaboration (G.L. Bayatian *et al.*), «CMS Physics Technical Design Report, Volume II: Physics Performance», *J. Phys. G: Nucl. Part. Phys.* **34**, 995 (2007).
[27] ATLAS Collaboration, «Expected performance of the ATLAS detector at the High-Luminosity LHC», ATL-PHYS-PUB-2019-005.
[28] CMS Collaboration (V. Khachatryan *et al.*), «Search for quark contact interactions and extra spatial dimensions using dijet angular distributions in proton–proton collisions at $\sqrt{s} = 8$ TeV», *Phys. Lett. B* **746**, 79 (2015).
[29] ATLAS Collaboration (G. Aad *et al.*), «Search for new phenomena in dijet mass and angular distributions from pp collisions at $\sqrt{s} = 13$ TeV with the atlas detector», *Phys. Lett. B* **754**, 302 (2016).
[30] CMS Collaboration (A.M. Sirunyan *et al.*), «Search for new physics with dijet angular distributions in pp collisions at $\sqrt{s} = 13$ TeV», *J. High Energy Phys.* **2017**, 013 (2017).
[31] FCC Collaboration (A. Abada *et al.*), «FCC Physics Opportunities: Future Circular Collider Conceptual Design Report Volume 1», *Eur. Phys. J. C* **79**, 474 (2019).
[32] FCC Collaboration (A. Abada *et al.*), «FCC-hh: The hadron collider: Future Circular Collider Conceptual Design Report Volume 3», *Eur. Phys. J. Spec. Top.* **228**, 755 (2019).
[33] M. Antonelli, M. Boscolo, R. Nardo, P. Raimondi, «Novel proposal for a low emittance muon beam using positron beam on target», *Nucl. Instrum. Methods Phys. Res. A* **807**, 101 (2016).
[34] D. Neuffer, V. Shiltsev, «On the feasibility of a pulsed 14 TeV c.m.e. muon collider in the LHC tunnel», *J. Instrum.* **10**, T10003 (2018).
[35] M. Boscolo, J. Delahaye, M. Palmer, «The Future Prospects of Muon Colliders and Neutrino Factories», *Rev. Accel. Sci. Technol.* **10**, 189 (2019).
[36] MICE Collaboration, «Demonstrations of cooling by the muon ionization cooling experiment», *Nature* **578**, 53 (2020).
[37] R. Ryne, «Muon colliders come a step closer», *Nature* **578**, 44 (2020).
[38] N. Amapane *et al.*, «LEMMA approach for the production of low-emittance muon beams», *Nuova Cim. C* **42**, 1 (2020).
[39] K.R. Long *et al.*, «Muon colliders to expand frontiers of particle physics», *Nat. Phys.* **17**, 289 (2021).
[40] K. Cheung, Z. Wang, «Physics potential of a muon–proton collider», *Phys. Rev. D* **103**, 116009 (2021).
[41] Y. Acar *et al.*, «Future circular collider based lepton–hadron and photon–hadron colliders: Luminosity and physics», *Nucl. Instrum. Methods Phys. Res. A* **871**, 47 (2017).
[42] G. Aydın *et al.*, «Contact interactions at future circular collider based muon–proton collider», *Acta Phys. Pol. B* **53**, 11-A3 (2022).
[43] V.I. Telnov, «A high-luminosity superconducting twin e^+e^- linear collider with energy recovery», *J. Instrum.* **16**, P12025 (2021).